Journal of Materials Chemistry A

ROYAL SOCIETY OF CHEMISTRY

COMMUNICATION

View Article Online
View Journal | View Issue

Cite this: J. Mater. Chem. A, 2024, 12, 29469

Received 12th September 2024
Accepted 7th October 2024

DOI: 10.1039/d4ta06493c

rsc.li/materials-a

Cascade co-polarized hydro-charged nanofibers enable long-term and harsh-environment-tolerant air filtration†

Xin Wang, [ab] Haoxin Liu,[a] Wang Cui,[a] Yuyao Li,*[a] Xiaoyang Guan[b] and Yong Liu *[a]

Particulate matter, along with outbreaks of infectious disease, has created a high demand for air filtration materials for personal protection. However, mainstream electret melt-blown filters suffer from both structural defects at the micron diameter scale and the technical drawback of separate processes for fiber forming and charging, failing to remove particles effectively and durably. Herein, cascade polarized nanofibrous membranes are constructed *via* an *in situ* hydro-charging strategy. Based on a creative perspective of high-speed electrospinning jets having a friction electrification effect with pure water, both outer and inner hydro-charging methods are adopted, resulting in polyvinylidene fluoride (PVDF) nanofibers with micro- and macro-polarized structures. Benefitting from unique cascade polarization, PVDF hydro-charged electrospun fibers (HCEFs) exhibit high filtration efficiency towards $PM_{0.3}$ (99.43%), a low pressure drop (41.7 Pa) and high surface potential (6037 V). HCEFs also show stable filtration performance when exposed to acid vapor, alkali vapor, and a high-humidity environment. This strategy may shed light on preparing next-generation high-performance electret filtration materials.

1. Introduction

Particulate matter (PM) has always accompanied the development of urbanization and industrialization, posing a huge threat to both the natural environment and human health.[1,2] Moreover, particles may breed various viruses and bacteria, which would be easily inhaled and cause deadly diseases. The just-concluded global coronavirus disease pandemic calls for the urgency of fabricating individual protective equipment and core air filtration materials.[3–5] To date, air filtration materials derived from nonwoven fibers are widely used to combat particulate pollution and to isolate the spread of viruses.[6] Among them, melt-blown fibers have become mainstream owing to their relatively small diameter and pore size, highly porous structure, and effective processing technology, endowing them with the ability to capture particles and promote air flow, namely the balance between filtration efficiency and pressure drop.[7] However, these structural advantages can only contribute to mechanical filtration behaviour, leading to a limitation in improving filtration performance. Therefore, electret technology has been introduced in the fabrication of air filter media, yielding electret melt-blown fibers that can capture particles due to both structural and electret effects. Attributed to the negligible influence of the electret effect on air flow and its remarkable contribution to particle capture, electret melt-blown fibers are considered a preferred material for high-performance air filters.

Traditional electret technologies mainly include corona charging, friction charging, and induction charging. Among them, corona charging is widely used, and in particular, corona-charged melt-blown polypropylene (MBPP) fibers have become a major raw material for personal protective equipment.[8,9] Zhang *et al.* prepared an electret MBPP air filtration material using a corona method, and its filtration efficiency was improved by 41.03% after being charged, while maintaining an air resistance of 52.9 Pa.[10] An important topic focusing on corona-charged fibers is the addition of electret masterbatches, which could further enhance charge capacity. For example, Guzhova *et al.*,[11] Lou *et al.*,[12] and Jiang *et al.*[13] added $BaTiO_3$, TiO_2, magnesium stearate and SiO_2, respectively, to improve the surface potential of electret melt-blown fibers, and all of them obtained materials with higher filtration performance. However, suffering from the micro-sized melt-blown fibers and post-processing charging process, corona electret fibers can only have shallow trapped charges, which tend to be neutralized or escape under the influence of a high-humidity environment.[14–16] Several studies have also worked to address this issue. Dou *et al.* have prepared an electro-blown spun electroactive nanofibrous membrane with excellent durability

[a]School of Textile Science and Engineering, Key Laboratory of Advanced Textile Composite Materials of Ministry of Education, Tiangong University, Tianjin 300387, China. E-mail: liyuyao@tiangong.edu.cn; liuyong@tiangong.edu.cn

[b]School of Fashion and Textiles, The Hong Kong Polytechnic University, Hung Hom, 999077, Kowloon, Hong Kong SAR, China

† Electronic supplementary information (ESI) available. See DOI: https://doi.org/10.1039/d4ta06493c

in a high-humidity environment.[17] Chen *et al.* also produced a moisture-induced electroactive nanofiber membrane to solve this problem, which demonstrated great filtration performance and moisture resistance.[18] Recently, hydro-charging technology, acknowledged as a stable method of charge storage, has received extensive attention. For a typical hydro-charging process, high-speed water jets are sprayed onto melt-blown fibers, resulting in stable friction charges that can resist high-humidity applications.[19,20] Some studies have explored the optimal process conditions and factors influencing hydro-charging for MBPP electret fabrics.[21,22] Notably, Zhang *et al.* fabricated a hydro-charged MBPP with a filtration efficiency of 99.84%, and the filtration efficiency only showed a decrement of 0.35% after depolarization processing and standing for two years.[23] This demonstrates the charge stability and long-term serviceability of hydro-charged melt-blown fibers. Hydro-charging technology offers new perspectives to improve the charge storage stability of electret fibers. However, there are still structural bottlenecks in the form of the large micro-sized diameter, as well as technological bottlenecks of separate fiber forming and charging processes. Hence, developing fine fibers and *in situ* electret technology is of great significance for obtaining electret fibers with maximum efficacy.

Electrospinning technology, featuring the use of high voltage while producing fine fibers, is an *in situ* charging method to produce electret nanofibers in one step. Electrospun electret fibers have the structural merits of a small diameter, small pore size and high porosity, which are expected to overcome the drawbacks of melt-blown electret fiber materials.[24,25] Currently, research on electrospun electret fibers is mainly devoted to enhancement of the charge effect. The most common strategy is to introduce nanoparticles into the spinning solution, such as boehmite, SiO_2, Si_3N_4, or Fe_3O_4.[26–29] However, the inherent agglomeration characteristic of nanoparticles triggers three problems for developing high-performance electrospun electret fibers: (i) ease of inhalation by humans poses an additional threat to human health;[30] (ii) the contribution of individual particles to the electret effect of the fibers is sacrificed to some extent;[31] (iii) agglomerated particles can serve as a pathway for moisture, leading to sensitive performance in hazy weather, to the breathing micro-environment (usually $\geq$80% RH) or to organic vapors in workshops.[32] Researchers have found that the surface potential retention of electrospun electret fibers decreased dramatically from 94.7% to 23.7% within 5 h when the humidity of the environment in which they were used was increased from 45% to 85%.[33] Therefore, developing electrospun fibers with an enhanced and permanent electret effect independent of particle charge enhancers remains a critical challenge.

Herein, we reported a strategy to fabricate cascade co-polarized *in situ* hydro-charged nanofibers with a stable electret effect and long-term filtering performance, which ingeniously exploited the constitutive relationship between high-speed electrospinning jets, a high-voltage electric field and pure water. Specifically, hydro-charged electrospun PVDF fibers were prepared *in situ* by simply regulating the environmental humidity (outer hydro-charging method) and water content in solvent (inner hydro-charging method) during the electrospinning process. The resulting fibers presented both microscopic dipoles from self-polarization of PVDF and macroscopic dipoles from porous spherical structures, contributing to an efficient $PM_{0.3}$ capture performance and high surface potential without any charge enhancer. Moreover, they demonstrate the ability to tolerate harsh environments, maintaining a stable filtration performance even when exposed to acid vapor, alkali vapor, or high-humidity conditions.

2. Results and discussion

2.1 Design of hydro-charged electrospun fibers

In order to prepare HCEFs with superior filtration performance and long-term service, our design is based on the following principles: (1) the HCEFs should be obtained *via* a facile, controllable and efficient method. (2) the HCEFs should exhibit a remarkable electret effect, requiring them to possess both polymer chain polarization and fiber caves for charge trapping.

The fabrication process of the hydro-charged electrospun fibers used in this work is shown in Fig. 1. To satisfy the first requirement, the preparation of the HCEFs is achieved by combining electrospinning and hydro-charging in one step, while the outer and inner hydro-charging was performed simultaneously to obtain electret fibers in a simple and efficient way. The second criterion was fulfilled by the formation of a cascade co-polarized structure. Under a water-enhanced electric field, the PVDF chains form a dipole orientation and generate microscopic dipoles, while the fiber membrane generates a porous spherical structure exhibiting macroscopic dipoles.[34] The cascade co-polarized structure collectively contributes to the excellent electret effect as well as the stable particle capture performance. Additionally, contact electrification generated between the high-speed flying PVDF polymer jets and charged water droplets contributes a portion of the surface charges.[35]

2.2 Outer hydro-charging enabled electret fibers with microscopic dipoles

Outer hydro-charging is achieved by adjusting the humidity during electrospinning, which mainly affects the morphological structure and charging effect of electret fibers. The scanning electron micrograph (SEM) images in Fig. 2a–c display the PVDF fibrous assemblies obtained from RH of 30%, 55%, and 80%. It can be seen that the fiber profile was uniform and smooth at 30% RH. At 55% RH, bead-like structures began to appear in the fiber aggregates. When the relative humidity was increased to 80%, bead-like structures were still present on the fibers, while the fibers had a curled shape. The average fiber diameters of PVDF-30, PVDF-55 and PVDF-80 are shown in Fig. 2d. The average fiber diameter was reduced from 193.07 nm to 113.98 nm when the humidity was increased from 30% RH to 55% RH. When the humidity was increased to 80% RH, the average diameter slightly decreased to 110.39 nm. As the environmental humidity increases, the number of water molecules in the confined space increases, leading to an increase in the

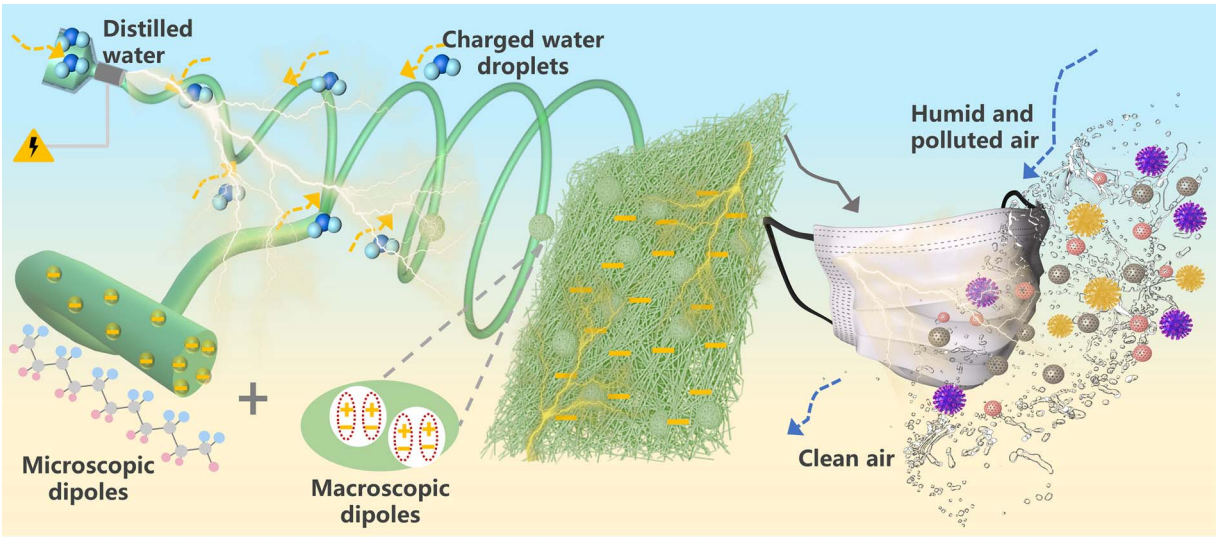

Fig. 1 Schematic diagram describing the concept of fabricating cascade co-polarized hydro-charged nanofibers.

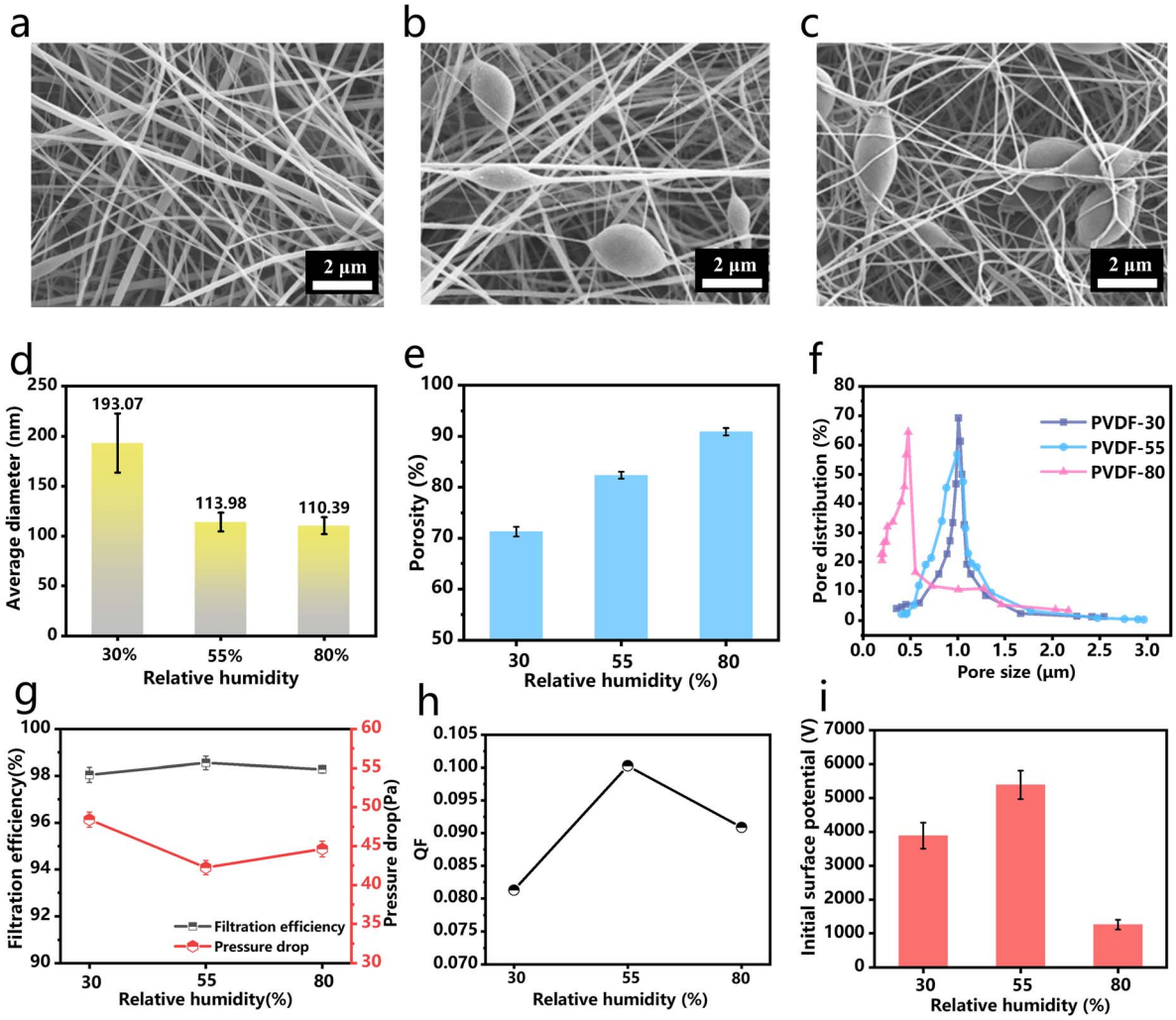

Fig. 2 SEM images of PVDF with various relative humidities of (a) 30%, (b) 55% and (c) 80%. (d) Fiber diameter distribution. (e) Porosity. (f) The distribution of pore size. (g) Filtration performance and (h) quality factor of PVDF nanofibers fabricated at different relative humidities. (i) Surface potential of PVDF nanofibers obtained from different relative humidities.

electric field intensity around the spinning needle. At the same time, the proliferation of water molecules enhances solvent evaporation, attributed to the compatibility between polar water molecules and the non-polar solvent DMF.[36] Consequently, when the humidity increases, the balance of electrostatic repulsion, viscoelastic force and surface tension in electrospinning is disrupted. This can affect the formation and stability of the Taylor Cone, which can cause some of the solution aggregates to form bead-like structures when the solution is not out of the jet trajectory. As the beads are formed, this leads to stretching of the fibers between the beads, which results in a reduction in the diameter of the fibers. At the same time, the increase in humidity also leads to an increase in the porosity of the fibers (Fig. 2e) and the average pore size is decreased (Fig. 2f). The combination of small fiber diameter and high porosity assists in the passage of airflow during filtration and reduces the pressure drop. According to a filtration performance test (Fig. 2g), the variation in filtration efficiency was negligible. However, the pressure drop of PVDF-55 is 42.2 Pa and that of PVDF-80 is 44.6 Pa, both lower than the pressure drop of PVDF-30 (48.4 Pa). Additionally, PVDF-55 exhibits the highest QF of 0.1003 (Fig. 2h). Despite the expectation that optimizing the fiber structure would lead to better filtration performance based on the mechanical filtration mechanism, the testing results indicate that PVDF-55 outperforms PVDF-80. Therefore, electrostatic adsorption may play a dominant role during filtration. The generation of electrostatic adsorption is provided by the fiber charging effect during electrospinning. The charging effect may be contributed by charges trapped on the surface and inside of the fibers during fiber formation and the orientation of polymer chain dipoles under the influence of an electric field. Therefore, the above phenomena indicate that the moisture content of the environment may have a significant influence on the charging effect.

To further investigate the charging effect of the PVDF fiber membrane, the initial surface potential of the fibers was tested, as shown in Fig. 2i. The initial surface potential was measured following a stabilization period of 30 min after completion of the electrospinning process. When the humidity was increased from 30% to 55%, the surface potential increased from 3890 V to 5390 V. However, when the humidity continued to increase to 80%, the surface potential of the fiber membrane decreased to 1255 V. This trend in surface potential of the fiber membrane under different amounts of humidity was consistent with the filtration performance. To reveal the contribution of water to the charging effect, the distribution of water molecules in an electric field was simulated using COMSOL software, as shown in Fig. 3a. By comparing the changes in electric field intensity around the needle in environments without and with moisture (55% RH), we observed that the red range at the needle tip expands and deepens when water molecules enter the electric field, indicating increased electric field intensity. Simultaneously, the water molecules dispersed around the needle also exhibit a strong electric field intensity, thereby increasing the electric field intensity in a larger space around the needle. Aided by water-molecule-enhanced electric field intensity, an increasingly apparent β-phase was found from PVDF-30, to PVDF-55 and PVDF-80 fibers, which was evidenced by the XRD spectra in Fig. 3b. Compared with PVDF powder, which exhibits three prominent peaks at $2\theta = 18.5°$ (020), 19.9° (110) and 26.5°

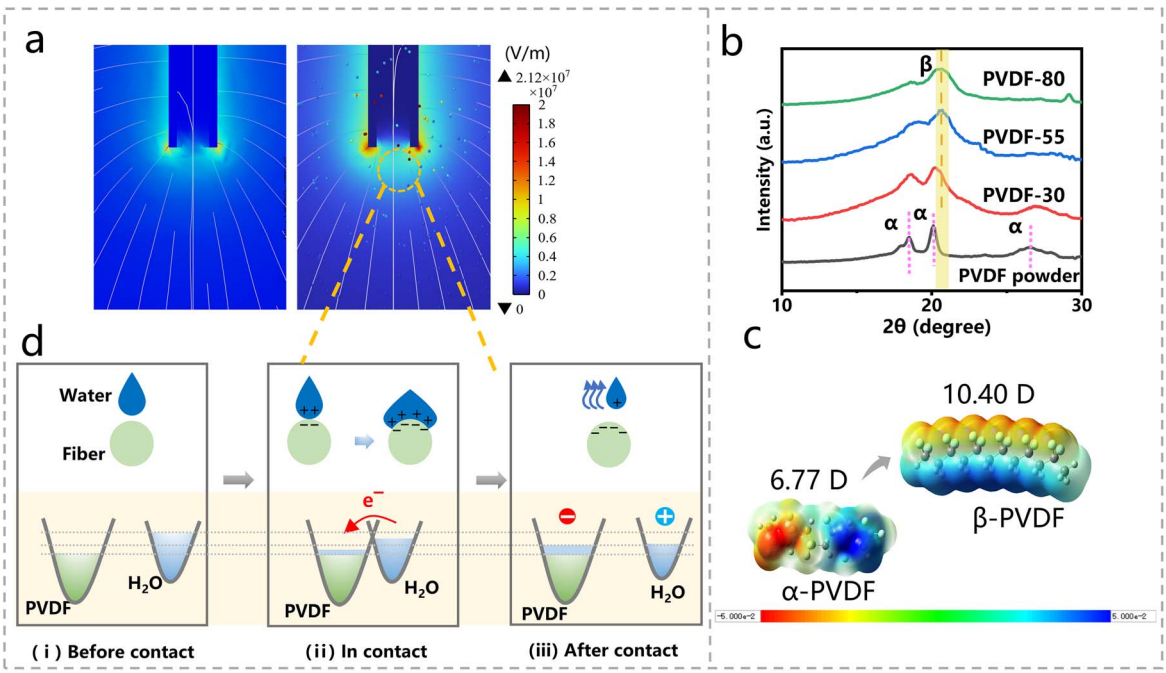

Fig. 3 (a) The electrostatic field distribution around the electrospinning needle without condensation of water molecules and with condensation of water molecules. (b) XRD patterns of PVDF nanofiber obtained from different relative humidities. (c) The dipole moment vectors and ESP-mapped electron densities for the α-PVDF and β-PVDF conformations. (d) The electron-cloud-potential-well model proposed for explaining the charge transfer between PVDF and H_2O.

(021), ascribed to crystal planes of α-phase PVDF, XRD spectra of PVDF-30, PVDF-55 and PVDF-80 indicated a gradual displacement of the α-phase by the β-phase ($2\theta = 20.6°$).[37,38] This distinct phase transition in PVDF-55 and PVDF-80 was attributed to the self-polarization of the PVDF chains by an enhanced electric field from the water effect and the powerful stretching force during electrospinning. As the β-phase of PVDF has a higher dipole moment of 10.4 D (Fig. 3c), it contributes to a higher surface potential to the PVDF fiber membranes.[39]

Simultaneously, the PVDF polymer jet flying at high speed in the electric field would come into contact with H_2O, and the contact electrification mechanism resulting from this contact is illustrated in Fig. 3d. This phenomenon also brings an increased charge to the fiber membrane. In the scenario where PVDF and H_2O are distinct, charge transfer is impeded because of the overlarge interface distance (Fig. 3d(i)), with no overlapping areas between the electron clouds of the two. When H_2O comes into contact with PVDF, electron clouds on their surface start to overlap, facilitating electrons hopping to the surface state of PVDF (Fig. 3d(ii)). After contact, the induced electrons remain on the surface states of PVDF (Fig. 3d(iii)).[40,41] As a result, PVDF will become negative with received electrons, while H_2O will become positive with lost electrons.[34] However, when the environmental humidity is maintained at 80% during the electrospinning process, a great reduction in the surface potential of the fiber membrane is observed. This is due to the fact that PVDF-80 is subjected to high humidity for a long period of time until the end of spinning, and the excessive H_2O promotes charge mobility on the electret fibers, leading to the charge escaping and the surface charge dissipating.

2.3 Inner hydro-charging enabled electret fibers with macroscopic dipoles

To further enhance the electret property of PVDF-55 fibers with microscopic dipoles, as well as to bestow upon them charge stability, an inner hydro-charging strategy was used to enable

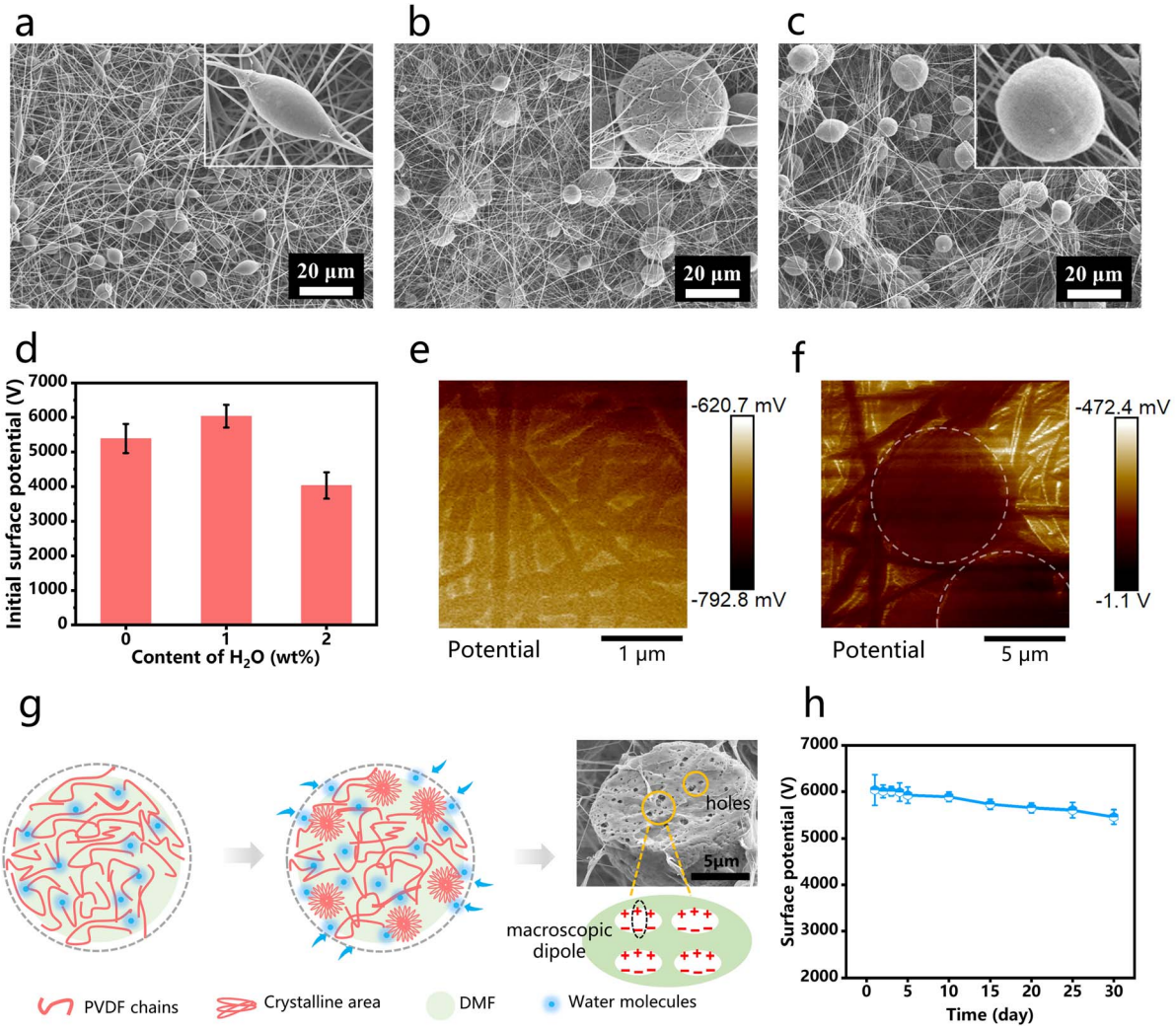

Fig. 4 SEM images of PVDF with various water contents in solvents of (a) 0 wt%, (b) 1 wt%, (c) 2 wt%. (d) Surface potential of PVDF nanofibers obtained from different contents of water within solutions. KPFM-measured surface potential of the PVDF fiber surface (e) without hydro-charging, (f) with hydro-charging. (g) The formation process of porous spheres and macroscopic dipoles during electrospinning. (h) Charge stability of PVDF-55@1 for 30 days.

the formation of macroscopic dipoles. Experimentally, the fiber structure was adjusted by adding distilled water to the PVDF precursor solution. Fig. 4a–c exhibit SEM images of hydrocharged PVDF-55 fibers with H_2O contents of 0, 1, and 2 wt%. When distilled water was mixed into the solvent, hydrophobic PVDF chains tended to rapidly agglomerate, resulting in a reunited spherical structure during the spinning process. Another more important change was the appearance of numerous holes on the surface of the spherical structure with a water content of 1 wt%, as shown by Fig. 4b. This may be due to the spherical structure containing H_2O molecules, which then in the electric field during electrospinning the water evaporates and the PVDF crystallizes, resulting in a large number of holes, as shown in Fig. 4g. At the same time, due to the symmetry of a charged sphere, a more uniform electric field can be generated compared to a bead-shaped one.[41] Additionally, Fig. 4c shows the fiber membrane with a large number of solid spherical structures with a smooth surface, fewer fibers and larger voids, which is mainly due to the plasticizing effect of the polymer caused by excess H_2O (2 wt%). Furthermore, the excessive amount of H_2O (>2 wt%) in the solvent can make it difficult to extrude the solution from the needle during spinning.

Benefiting from the coupled effect of outer and inner hydrocharging, the surface potential of the PVDF-55@1 fiber membrane achieved up to 6037 V (Fig. 4d). This increased surface potential might come from the formation of numerous holes, as indicated by the microscopic surface potential of fibers and porous spheres displayed in Fig. 4e and f. The KPFM image shows that the surface of the porous spheres has a dark brown color, while the fiber surface appears yellow, indicating that the porous spheres have a higher potential than the fibers. The increase in potential of the porous spheres may be due to the air inside the holes generating Paschen breakdown,[42] resulting in a large number of ordered macroscopic dipoles being formed inside the holes (Fig. 4g). However, the surface potential of the PVDF fiber membranes did not improve consistently when the water content increased to 2 wt% but decreased. This phenomenon might be attributed to the disappearance of holes on the spherical structure, also confirming the significant role of macroscopic dipoles in improving the electret effect. At the same time, due to the enlarged contact area between PVDF and H_2O, CE occurs between the inner water, outer water and the PVDF when the jet flies out of the needle. Then, the charge is captured both within and on the surface of the fiber during fiber formation, resulting in an enhanced charge storage capacity.[43–45] Charge stability was also investigated under indoor storage for 30 days (Fig. 4h) with a room temperature of 25 ± 3 °C and a relative humidity of 60 ± 5% RH, and the surface potential still remained at 5400 V.

2.4 Moisture and chemical resistance performance of hydrocharged electrospun fibers

Considering the application scenarios for filters, such as breathing micro-environments (with an RH from 80 to 90%) for respiration filters, fog and hazy weather (with an RH of 80–95%)[46] or organic vapours in factories, humidity is often an unavoidable factor affecting the stability and durability of filters. Therefore, the charge stability of fiber membranes under conditions of high humidity has been tested. Fig. 5a–d depicts

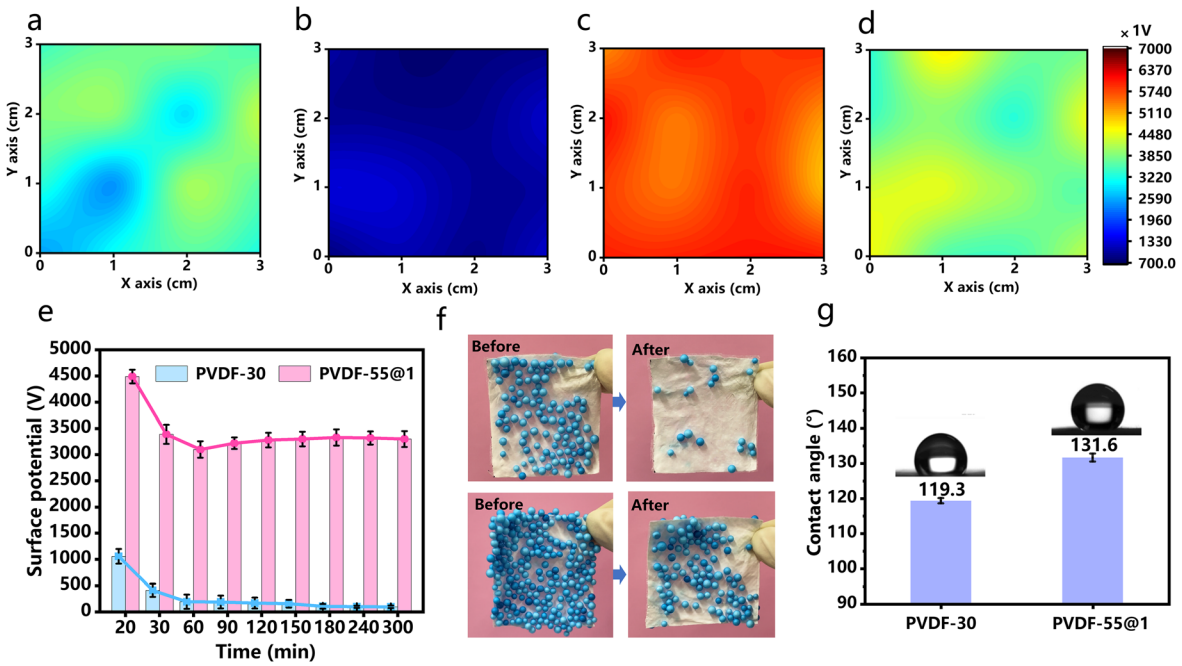

Fig. 5 Surface potential distribution images of PVDF-30 (a) before and (b) after wet treatment at 90% RH. Surface potential distribution images of PVDF-55@1 (c) before and (d) after wet treatment at 90% RH. (e) Surface potential decay of PVDF-30, PVDF-55@1 fibers under 90% RH for 300 min. (f) Effect of electrostatic adsorption of foam balls before and after wet treatment of PVDF-30 (top), PVDF-55@1 (bottom) fibers. (g) The mean contact angles of the PVDF-30, PVDF-55@1 surfaces.

the surface potential distribution of the electret fiber membranes before and after exposure to a 90% humidity environment for 20 min. It is observable that the surface potential of PVDF-55@1 was uniformly distributed with an average potential of 6000 V, which then decreased to 4500 V after wet treatment. However, the PVDF-30 membrane directly declined from 4000 V to 1000 V, showing inferior moisture resistance to PVDF-55@1.

In a further evaluation of long-term stability, Fig. 5e demonstrates the variation in surface potential of PVDF-30 and PVDF-55@1 at 90% RH for 300 min. The surface potential of PVDF-30 decreased continuously from 1058 V to 98 V after wet treatment, with a significant decay rate of 90.73%. However, PVDF-55@1 exhibited a decay rate of 26.50% after wet treatment, and the surface potential was still maintained at 3300 V. The surface potential of the PVDF-55@1 membrane decayed during the initial 60 min of wet treatment, due to dissipation of unstable charges on the surface of the fiber membrane. Then the surface potential was maintained at 3300 V, which can mainly be attributed to the stable charge storage capacity due to the cascade co-polarization. First, PVDF as a ferroelectret could polarize under the action of an electric field, resulting in stable dipole charges stored inside the fiber.[44,47] Subsequently, the porous structure of ferroelectric electret has been shown to have good charge storage stability, where the charge can be stored inside the cavity without being dissipated by the external environment.[48,49] Therefore, with the combined effect of microscopic dipole charges and macroscopic dipoles in the porous structure, the PVDF-55@1 fiber membrane exhibits stable electrostatic properties. Moreover, the piezoelectric properties of the fiber membrane are demonstrated in Fig. S1,† which also exhibits good piezoelectric responsivity. Subsequently, a comparison of the electrostatic adsorption capacity and charge stability of PVDF-30 and PVDF-55@1 was conducted through foam ball adsorption experiments to provide a more intuitive analysis. Fig. 5f shows that foam balls were firmly adsorbed on the two fiber membranes before wet treatment, but more foam balls were adsorbed on PVDF-55@1.

After wet treatment for 300 min, the number of foam balls adsorbed on PVDF-55@1 was still 104, while there were only 19 on PVDF-30. These results indicate that PVDF-55@1 showed superior charge storage capacity and moisture stability. Fig. 5g characterizes the hydrophobicity of the fibers with the water contact angle measurements. The results showed that PVDF-55@1 had an average contact angle of 131.6° and possessed enhanced hydrophobicity over PVDF-30. The hydrophobic fiber membrane surface impedes the penetration of water molecules deeper into the fiber structure, thus dissipating the charges, which also enhances the ability of PVDF-55@1 to resist moisture.

According to a filtering performance test (Fig. 6a), PVDF-55@1 shows enhanced $PM_{0.3}$ removal efficiency of 99.43%, and a pressure drop of 41.7 Pa. Fig. 6b demonstrates the excellent resistance of HCEFs to strong acid and alkali solutions while maintaining their complete structural integrity. Moreover, a self-designed PM filter was used to simulate a chemical vapor environment (Fig. 6c) to investigate the filtration performance. Fig. 6d and e demonstrate the filtration efficiency of HCEFs before and after 5 h of acid and alkaline vapor treatment, respectively. The results show that the filtration efficiency

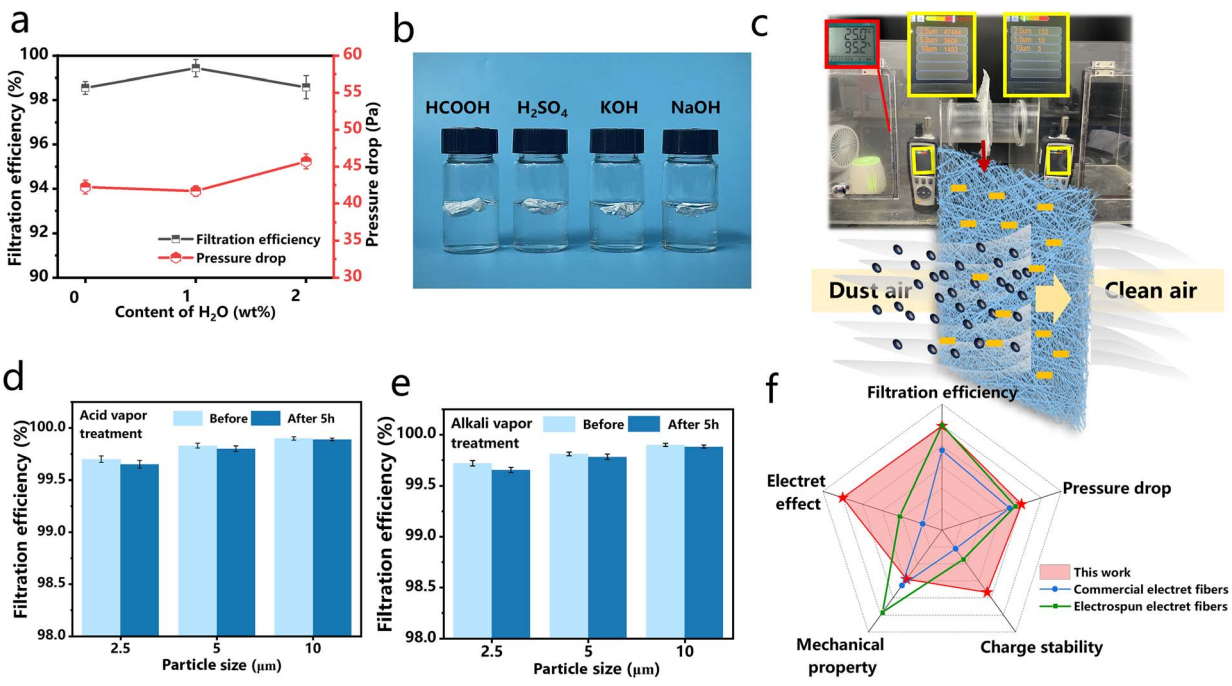

Fig. 6 (a) Filtration performance of HCEFs. (b) Chemical stability of fibers against acids or alkalis. (c) Self-designed PM filter. The filtration efficiency of different particles for HCEFs after (d) acid and (e) alkali treatments. (f) Radar chart comparing the comprehensive performance of the HCEFs with commercial electret fibers and electrospun electret fibers.

of the hydro-charged electrospun fibers remains unchanged after acid or alkali treatment, indicating their excellent chemical resistance performance. As qualitatively shown in Fig. 6f, the comparative benefits of HCEFs, in relation to existing commercial electret filters and earlier investigations into electrospun electret fibers, were underscored. Specific comparative data is shown in Fig. S2 and Table S1.† The filtration performance and electrostatic properties of HCEFs are optimized simultaneously, maximizing the advantageous structural effect from electrospinning and the superb electret effect from hydro-charging. With this benefit, HCEFs have become an effective way to overcome the limitations of enhancing air filtration material performance. Meanwhile, the superior charge stability gives the filter materials a longer service life, and their resistance to moisture and chemicals provides them with a wider range of applications. However, based on the inherent structural limitations of electrospinning, the mechanical properties are slightly inferior to those of other melt-blown electret fibers. This problem can be solved by using HCEFs as a core layer or multilayer film composite. With their wide range of environmental tolerance, HCEFs are suitable for use as a core layer in respiratory masks, purifiers, and similar applications.

3. Conclusions

Cascade co-polarized PVDF nanofibers were successfully electrospun using proposed *in situ* outer hydro-charging and inner hydro-charging strategies for efficient air filtration. Outer hydro-charging was conducted by adjusting the environmental humidity during electrospinning, and the results indicated that 55% RH promoted the dipole orientation of the PVDF polymer chains, which were considered as microscopic dipoles. Additionally, inner hydro-charging was operated by adding pure water in solvent, and it was found that 1 wt% water content yielded a fiber structure with porous beads, which could serve as macroscopic dipoles. Benefitting from the hydro-charging strategy and cascade co-polarized feature, the resultant PVDF electrospun fibers had a high surface potential of 6037 V, enhanced $PM_{0.3}$ removal efficiency of 99.43% and a low pressure drop of 41.7 Pa. Moreover, the surface potential after high-humidity treatment for 300 min exhibited a decay rate of only 26.50%, and there was no significant change in filtration efficiency after chemical moisture treatment. Therefore, HCEFs are perfectly suited for use in personal prospective equipment, with their good resistance to high humidity and acidic and alkaline environments also being verified. This approach provides a new strategy for the preparation of hydro-charged fibers, and future work will continue to expand the field of applications based on their charge properties.

4. Experimental section

4.1 Materials

Polyvinylidene fluoride (PVDF, purity: 99.99%, $M_w = 570\,000$, Solvey Co., Ltd, Belgium) powder, *N*,*N*-dimethylformamide (DMF, Shanghai Macklin Biochemical Co., Ltd, China), distilled water; formic acid (HCOOH), sulfuric acid (H_2SO_4), potassium hydroxide (KOH), and sodium hydroxide (NaOH) were all procured from Macklin Co., Ltd (Shanghai, China). The commercial electret fiber used for comparison was the 3 M electrostatic electret filter.

4.2 Preparation of PVDF hydro-charged electrospun fibers

First, a 20 wt% PVDF solution was prepared by dissolving 2.0 g of PVDF polymer powder in 8.0 g of DMF under continuous stirring for at least 8 h at 80 °C. Subsequently, the PVDF fibers were prepared using an electrospinning machine (Qingdao Nuokang Environmental Protection 96 Technology Co. Ltd, China) under a stable applied voltage of 20 kV, with feeding at a rate of 1 mL h^{-1}. The nanofibers were deposited onto a polyethylene nonwoven-encased (filtration efficiency: 5%, pressure drop: 0 Pa) grounded roller, positioned 15 cm away from the electrospinning needle, while rotating at a rate of 60 rpm. Throughout the electrospinning operation, the ambient temperature was meticulously maintained at 25 ± 2 °C. However, the relative humidity (RH) of the electrospinning was adjusted to 30 ± 3%, 55 ± 3%, and 80 ± 3%, resulting in PVDF-30, PVDF-55, and PVDF-80 electret fiber membranes, respectively. The humidity was simultaneously controlled by a humidifier and an exhaust air system to ensure the stability of humidity during spinning. Furthermore, 1 wt% and 2 wt% distilled water were introduced into DMF and stirred continuously for 30 min at room temperature. Furthermore, the PVDF powders were dissolved in the mixture of DMF and distilled water under continuous stirring for at least 8 h at 80 °C. The PVDF/H_2O electret fibers were fabricated following the above-mentioned methodology with a relative humidity of 55 ± 3%.

4.3 Characterization

The morphology and structure of the fibers were observed with a field-emission scanning electron microscope (SEM, TESCAN MIRA LMS, Tescan Ltd, Czech Republic). The measurement of the average fiber diameter was determined through a statistical evaluation of 100 fibers that were randomly selected and analyzed using ImageJ software for image analysis. The pore size distribution was analyzed with a bubble pressure method membrane pore size analyzer BSD-PB (BeiShiDe Instrument Co., Ltd, China). The porosity of the fibrous membrane (p) was calculated using the formula: $p = (1 - m/\rho SH) \times 100\%$, where ρ is the density of PVDF; m, S, and H represent the base weight, area, and thickness of the fiber network, respectively. The surface potential of the PVDF electret fiber membrane was measured using a non-contact electrostatic field meter EFM-022 (Kleinwachter, Germany). The tester was placed vertically 2 cm above three samples, and 10 sets of data were collected at different positions of each sample to calculate the average surface potential (the surface potential of the PVDF electret fibers is negative). The crystal phase structures of the PVDF electret fibers were tested using a Bruker XRD (D8 DISCOVER) instrument. The simulated electric field in electrospinning was calculated with commercial COMSOL software. Several water molecules with a radius of 5 μm were put in the environment. Calculations of the dipole moment and electrostatic potential of

PVDF were conducted by utilizing Gaussian 09 software. The water contact angles of the fiber membrane were measured with a contact angle tester (Powereach JC2000C, China). Noncontact mode KPFM (Bruker Dimension Icon, Germany) was used to directly measure the surface potential of the fiber. High-humidity treatment could be regulated *via* a humidifier placed in an enclosed test chamber, where the humidity was adjusted to 90% RH and then the fiber membrane was suspended in the test chamber. The mechanical properties of the membranes were evaluated with a tensile testing instrument HY-0580 (Shanghai HongYi Testing Instruments Co., Ltd, China).

4.4 Evaluation of air filtration performance

The filtration efficiency and pressure drop were assessed with a filter testing apparatus (LZC-K, Huada Filter Technology Co., Ltd, China). For aerosol generation, a 2 wt% sodium chloride (NaCl) solution was employed to create aerosols with a median diameter of 0.3 μm. The test area was 100 cm^2, and the NaCl aerosol flow rate was set at a rate of 32 L min^{-1}.

Data availability

The data supporting this article have been included as part of the ESI.†

Conflicts of interest

The authors have no conflicts of interest to disclose.

Acknowledgements

This work was supported by the National Natural Science Foundation of China (No. 52203048) and Tianjin and Ministry of Education Key Laboratory for Advanced Textile Composite Materials, Tiangong University. The authors also thank Shiyanjia Lab (**https://www.shiyanjia.com/**) for testing service.

References

1 X. D. Li, L. Jin and H. D. Kan, *Nature*, 2019, **570**, 437–439.
2 R. J. Laumbach and K. R. Cromar, *Annu. Rev. Public Health*, 2022, **43**, 293–309.
3 D. K. Yoo, H. C. Woo and S. H. Jhung, *Coord. Chem. Rev.*, 2020, **422**, 213477.
4 H. Liu, C. Y. Cao, J. Y. Huang, Z. Chen, G. Q. Chen and Y. K. Lai, *Nanoscale*, 2020, **12**, 437–453.
5 Y. Y. Shi, Y. F. Ji, H. Sun, F. Hui, J. C. Hu, Y. X. Wu, J. L. Fang, H. Lin, J. X. Wang, H. L. Duan and M. Lanza, *Sci. Rep.*, 2015, **5**, 6237–6245.
6 X. Wang, W. Cui, Y. Y. Li and Y. Liu, *Sep. Purif. Rev.*, 2024, **53**, 336–350.
7 Y. Kara and K. Molnár, *J. Ind. Text.*, 2022, **51**, 137S–180S.
8 G. S. Larsen, Y. Q. Cheng, L. L. Daemen, T. N. Lamichhane, D. K. Hensley, K. L. Hong, H. M. Meyer, S. J. Monaco, A. M. Levine, R. J. Lee, E. Betters, K. Sitzlar, J. Heineman, J. West, P. Lloyd, V. Kunc, L. Love, M. Theodore and M. P. Paranthaman, *ACS Appl. Polym. Mater.*, 2021, **3**, 1022–1031.
9 H. C. Gao, W. D. He, Y. B. Zhao, D. M. Opris, G. B. Xu and J. Wang, *J. Membr. Sci.*, 2020, **600**, 117879.
10 H. F. Zhang, J. X. Liu, X. Zhang, C. Huang and X. Y. Jin, *Rsc Adv.*, 2018, **8**, 7932–7941.
11 A. A. Guzhova, M. F. Galikhanov, Y. A. Gorokhovatsky, D. E. Temnov, E. E. Fomicheva, E. A. Karulina and T. A. Yovcheva, *J. Electrost.*, 2016, **79**, 1–6.
12 C. W. Lou, Y. H. Shih, C. H. Huang, S. A. Lee, Y. S. Chen and J. H. Lin, *Appl. Sci.*, 2020, **10**, 2686.
13 T. J. Jiang, G. S. Zeng, C. Hu, C. Meng and Y. Chen, *Fibers Polym.*, 2021, **22**, 957–963.
14 H. M. Xiao, Y. P. Song and G. J. Chen, *J. Electrost.*, 2014, **72**, 311–314.
15 Y. X. Zhao, Y. X. Zhang, J. G. Ju, Z. M. Qian, X. F. Cui, S. Y. Wang, B. W. Cheng and W. M. Kang, *Sep. Purif. Technol.*, 2024, **332**, 16554–16570.
16 Y. Cheng, W. Wang, R. R. Yu, S. K. Liu, J. Shi, M. J. Shan, H. T. Shi, Z. W. Xu and H. Deng, *Sep. Purif. Technol.*, 2022, **282**, 120030.
17 Y. J. Dou, N. Wang, S. H. Zhang, C. H. Sun, J. M. Chen, Z. H. Qu, A. H. Cui and J. W. Li, *J. Hazard. Mater.*, 2024, **469**, 134064.
18 J. M. Chen, S. H. Zhang, Y. J. Dou, G. T. Han, N. Wang, Z. H. Qu, C. G. Liu and J. W. Li, *Sep. Purif. Technol.*, 2024, **348**, 127772.
19 H. Gao, G. H. Liu, J. Guan, X. F. Wang, J. Y. Yu and B. Ding, *Chem. Eng. J.*, 2023, **458**, 141412.
20 Z. H. Pan, G. H. Liu, X. Y. Chen, A. A. Babar, Y. J. Dong and X. F. Wang, *J. Text. Inst.*, 2022, **113**, 2128–2134.
21 Z. Y. Wang, G. J. Chen, X. L. Hong, J. Y. Yu, J. F. Zhang, Y. K. Ding, Q. W. Lou and H. S. He, *J. Electrost.*, 2022, **116**, 103683.
22 J. F. Zhang, G. J. Chen, K. J. Zhang, D. Z. Zhao, Z. Y. Li and J. W. Zhong, *ACS Appl. Mater. Interfaces*, 2023, **15**, 2449–2458.
23 X. Zhang, Y. X. Wang, R. Y. Ni, H. F. Zhang, J. X. Liu, Y. Zhao and X. Y. Jin, *Sep. Purif. Technol.*, 2022, **303**, 122236.
24 J. J. Xue, T. Wu, Y. Q. Dai and Y. N. Xia, *Chem. Rev.*, 2019, **119**, 5298–5415.
25 X. Wen, J. Xiong, S. L. Lei, L. M. Wang and X. H. Qin, *Adv. Fiber Mater.*, 2022, **4**, 145–161.
26 X. Yang, Y. Pu, S. X. Li, X. F. Liu, Z. S. Wang, D. Yuan and X. Ning, *ACS Appl. Mater. Interfaces*, 2019, **11**, 43188–43199.
27 R. X. Xu, J. Y. Feng, L. X. Zhang and S. Q. Li, *Sep. Purif. Technol.*, 2022, **303**, 122224.
28 F. Liu, M. Y. Li, W. L. Shao, W. L. Yue, B. J. Hu, K. Weng, Y. K. Chen, X. Liao and J. X. He, *J. Colloid Interface Sci.*, 2019, **557**, 318–327.
29 X. Y. Song, G. Q. Cheng, B. W. Cheng and J. F. Xing, *J. Mater. Res.*, 2016, **31**, 2662–2671.
30 M. A. Zoroddu, S. Medici, A. Ledda, V. M. Nurchi, J. I. Lachowicz and M. Peana, *Curr. Med. Chem.*, 2014, **21**, 3837–3853.
31 Y. Y. Li, X. Yin, Y. Si, J. Y. Yu and B. Ding, *Chem. Eng. J.*, 2020, **398**, 125626.
32 C. Liu, Z. J. Dai, B. He and Q. F. Ke, *Materials*, 2020, **13**, 4774.

33 H. J. Kim, S. J. Park, D. I. Kim, S. Lee, O. S. Kwon and I. K. Kim, *Sci. Rep.*, 2019, **9**, 7015.
34 F. P. Wang, Z. F. Xia, X. Q. Zhang, J. F. Huang and J. Shen, *Acta Phys. Sin.*, 2007, **56**, 6061–6067.
35 Y. Nan, J. J. Shao, M. Willatzen and Z. L. Wang, *Research*, 2022, **2022**, 2639–5274.
36 N. B. Cheng, D. Y. Miao, C. Wang, Y. Y. Lin, A. A. Babar, X. F. Wang, Z. H. Wang, J. Y. Yu and B. Ding, *Chem. Eng. J.*, 2023, **460**, 141581.
37 K. Ibtehaj, M. H. H. Jumali and S. Al-Bati, *Polymer*, 2020, **208**, 122956.
38 J. Y. Hu, Y. D. Zhu, H. L. Zhang, Y. Y. Gu and X. D. Yang, *Smart Mater. Struct.*, 2017, **26**, 085019.
39 H. Liu, S. C. Zhang, L. F. Liu, J. Y. Yu and B. Ding, *Adv. Funct. Mater.*, 2020, **30**, 1616–3028.
40 C. Xu, Y. L. Zi, A. C. Wang, H. Y. Zou, Y. J. Dai, X. He, P. H. Wang, Y. C. Wang, P. Z. Feng, D. W. Li and Z. L. Wang, *Adv. Mater.*, 2018, **30**, 1521–4095.
41 F. Zhan, A. C. Wang, L. Xu, S. Q. Lin, J. J. Shao, X. Y. Chen and Z. L. Wang, *ACS Nano*, 2020, **14**, 17565–17573.
42 A. L. Bozic, *Soft Matter*, 2018, **14**, 1149–1161.
43 R. A. Kurniawan and P. P. J. Chu, *J. Macromol. Sci., Part B: Phys.*, 2023, **62**, 738–754.
44 P. Saxena and P. Shukla, *Adv. Compos. Hybrid Mater.*, 2021, **4**, 8–26.
45 Z. Q. Liu, Y. Z. Huang, Y. X. Shi, X. L. Tao, H. Z. He, F. D. Chen, Z. X. Huang, Z. L. Wang, X. Y. Chen and J. P. Qu, *Nat. Commun.*, 2022, **13**, 2041–1723.
46 Y. C. A. Yang, B. Z. Ge, X. S. Chen, W. Y. Yang, Z. J. Wang, H. S. Chen, D. H. Xu, J. H. Wang, Q. X. Tan and Z. F. Wang, *Atmos. Res.*, 2021, **256**, 0169–8095.
47 C. S. Guo, H. T. Shi, W. Wang, X. Y. Pei, K. Y. Teng, Y. L. Hu, Z. W. Xu, H. Deng and X. M. Qian, *Sci. Total Environ.*, 2020, **722**, 0048–9697.
48 N. Z. Wang, M. A. Baferani, R. Daniels, C. Wu, J. D. Huo, J. van Turnhout, G. A. Sotzing, R. Gerhard and Y. Cao, *J. Phys. D: Appl. Phys.*, 2024, **57**, 1361–6463.
49 Z. Xia, A. Wedel and R. Danz, *IEEE Trans. Dielectr. Electr. Insul.*, 2003, **10**, 102–108.

